Screening of charged impurities in graphite intercalation compounds

M. F. Lin and Kenneth W.-K. Shung
Physics Department, National Tsing Hua University, Hsinchu, Taiwan 30043, Republic of China
(Received 17 March 1992; revised manuscript received 12 June 1992)

The screening problem has been studied here with the use of an analytically expressed dielectric function, which was calculated in accordance with the band structure of the graphite intercalation compounds. Due to the special band structure of this system, the screening has been found to be very effective at short distances from an impurity, and a strong but short-period Friedel oscillation also exists at large distances. These features are expected to have important effects on, for example, the resistivity and the ordering of impurities in the system. We have calculated the residual resistivity due to the scattering from charged impurities. Direct comparison with measured results has indicated that a small amount of such impurities could explain the observed resistivities in the stage-1 C_8M compounds (M for K, Rb, and Cs).

I. INTRODUCTION

Graphite intercalation compounds (GIC's) are very interesting systems and have attracted many recent investigations.[1,2] Upon intercalation, electrons are either transferred to (from) the carbon layer from (to) the intercalants. The Fermi level of GIC's can, as a result, be adjusted by employing different intercalants. GIC's can achieve a conductivity as good as copper,[1] with the proper intercalations.

Although GIC's are good conductors, analytic studies on their screening properties are still lacking. The Lindhard dielectric function is well known for providing a basis of understanding for screening properties in metals. Unfortunately, the same dielectric function cannot be employed for GIC's, which have very special structures. First, graphite compounds are layered systems; the conductivity along the direction normal to the layers is smaller[1] by several orders of magnitude than that parallel to graphite layers. Second, the conduction and valence bands are degenerate at the U point in $\mathbf{k}$ space, where the state energy is proportional to $k=|\mathbf{k}|$, not the usual quadratic energy dispersion relation. The special band structure also suggests important contributions coming from the valence-to-conduction interband transitions.

Shung[3] developed for GIC's a dielectric function, which takes into account the layer structure and the special band structure of GIC's. The calculation has been treated exactly within the random-phase approximation (RPA) and the result expressed analytically. The dielectric function is therefore expected to work for GIC's in a fashion similar to what Lindhard's dielectric function does for simple metals. GIC's, in Shung's approach, are described by a superlattice model in which different graphite layers are coupled to each other by direct Coulomb interaction. The two-dimensional (2D) band structure of each graphite layer follows from a tight-binding calculation which yields the Blinowski's band structure[4] of the form

$$E_k^{c,v}=\pm v_f k \ , \tag{1}$$

where $v_f=2.13$ Åγ_0, and γ_0 is the resonance integral due to the nearest-neighbor coupling. The superscript c (v) represents the conduction (valence) band. Such a 2D band structure has been the basis of many studies— on both the acceptor- and the donor-type, stage-1 and stage-2 GIC's.[3,5–7] One great advantage of the present approach is that the complicated band structure of graphites can be included for analytic studies and the results be directly compared with measurements. It has been employed with success[3,5] in the study of plasmons and of other dielectric properties of GIC's.

Shung's dielectric function is used here to study the screening of charged impurities in GIC's. The impurities are put either on the carbon layer or on the intercalant layer. The effective potential and the induced charges are then derived analytically, which can be applied either to the donor- or to the acceptor-type GIC's. We choose to employ it to study the C_8M compounds (M stands for K, Rb, and Cs), since measured resistivities of these compounds are available for comparisons. Complication due to the intercalant-induced S bands has been neglected here. There are suggestions[6,7] that the rigid 2D bands are still available in these compounds. Modification due to the induced S bands will be studied elsewhere.

Our calculations illustrate that the band structure of GIC's plays an important role in screening. The interband transitions greatly enhanced the short-range screening; the finite size of the π bands introduced strong but rather short-period Friedel oscillations. The latter might have important effects on the impurity ordering. It should be emphasized that such band structure cannot be easily mimicked with, e.g., a superlattice of layers of 2D electron gas, which has also been calculated here for the purpose of comparison. In other words, one cannot properly understand the GIC's without paying due attention to its band structure. DiVincenzo and Mele[8] employed a similar band structure and studied the screening effect numerically. They also discovered the importance of the band structure in graphite, including a nonlinear screening effect that is absent in the present theory. It is noticed that they have studied the response of a single,

undoped (i.e., $E_F=0$) graphite layer. The nonlinear effect should be less important in our systems where E_F is about 1.5 eV and the coupling among the graphite layers is significant. The present linear response theory is expected to describe well the important screening behavior of low-stage GIC's. Other features of screening in GIC's have been discussed by many authors.[2,9]

The residual resistivity due to charged impurities is also studied here as a further illustration of the importance of the special GIC's structure. The Boltzmann equation can be directly used here to calculate the resistivity, since the screening properties of such impurities are now known. The special band structure of GIC's enhances the carrier mobility in two essential ways: one is that the effective mass of electrons is reduced, and the other is that the matrix element for backward scattering is also reduced. Reducing the strength of backward scattering clearly enhances the carrier mobility. The resistivities for stage-1 C_8M compounds are calculated here for specific comparisons. The measured resistivities[10] were found to be explained with about less than one impurity in every 10^5 carbon atoms. Such low impurity concentration seems reasonable here. A closer study in this regard, however, is necessary—with, e.g., impurities of known properties being doped into GIC's in a controlled manner. The present theory provides a basis for quantitative analysis in such future studies.

This paper is organized as follows. The screening of a charged impurity in GIC's is discussed in Sec. II. The residual resistivities of C_8M compounds are calculated and the results compared with measurements in Sec. III. Concluding remarks are made in Sec. IV.

II. THE IMPURITY SCREENING

The stage-1 GIC's have the superlattice structure of an infinite series of identical graphite layers with one intercalant layer sandwiched between two adjacent graphite layers. Some approximations are necessary for addressing the properties of such a complicated system. First of all, we employ Blinowski's band structure, so that we have the advantage of taking the band-structure effect into full consideration, and expressing the dielectric function in a compact form.[3] This is important for analytical discussion, and also for numerical studies. We further assume that intercalation merely alters the Fermi energy E_F in the rigid band described by Eq. (1). Finally, we neglect the electron hopping between different layers. The Coulomb interaction for electrons on different layers are, however, taken into consideration. Such a model is similar to that[11] used successfully for semiconductor superlattices. The difference in band structures is what distinguishes the two systems.

Let us first examine $\epsilon^{2D}(q)$, the static dielectric function of a single isolated graphite layer. Within the self-consistent field (SCF) treatment,[3] we can express

$$\epsilon^{2D}(q)=\epsilon_0-V_q X(q) , \tag{2}$$

where $X(q)=X_a(q)+X_b(q)$. $X_{a(b)}(q)$ is the response function due to the intraband (interband) transitions. We have calculated the response functions in detail[3] and a summary of the results has been given for easy references in the Appendix. ϵ_0 is the background dielectric constant due to all excitations outside the π band of the graphite. $V_q=2\pi e^2/q$ is the matrix element of the Coulomb interaction in two dimensions. We would like to emphasize that we have actually used the Bloch wave functions in evaluating the matrix element $X(q)$. Thus, the full band-structure effect of the complicated GIC's has been taken care of.

Equation (2) describes an isolated graphite layer. It is necessary, for GIC's, to take into account the coupling of electrons on different layers. By assuming that Bloch states are localized to the graphite layers, we find that the Coulomb interaction for electrons on layers l and l' is $V_{l,l'}(q)=V_q\exp\{-q|l-l'|I_c\}$; where I_c is the distance between two neighboring graphite layers.

The dielectric function is modified after the inclusion of the interlayer Coulomb coupling. For an external potential $V_l^{ex}(q)$ on the l layer, the total effective potential is[11]

$$\epsilon_0 V_l^{eff}(q)=V_l^{ex}(q)+\sum_{l'} V_{l,l'}(q)V_{l'}^{eff}(q)X(q) . \tag{3}$$

$V_{l'}^{eff}(q)X(q)$ is recognized to be the induced charge density $[n_{l'}^{in}(q)]$. Equation (3) can be easily solved by first performing the following Fourier transform:

$$\sum_l V_l^{ex}(q)e^{ik_z lI_c}=V^{ex}(q,k_z) , \tag{4}$$

where $|k_z I_c|\le\pi$; and similarly for $V_l^{eff}(q)$. The dielectric function is then expressed by[11]

$$\epsilon(q,k_z)=\epsilon_0-V_q S(q,k_z)X(q) , \tag{5}$$

where $S(q,k_z)=\sinh(qI_c)/[\cosh(qI_c)-\cos(k_z I_c)]$.

Our main concern in this study is the potential due to charged impurities. Let us consider one charged impurity Ze located at $(0,0,z)$. For convenience, we denote the first layer below the impurity $l=0$; thus, $0\le z<I_c$. The effective potential is expressed by

$$V_l^{eff}(q;z)=\frac{ZV_q}{\epsilon_0}\left\{\frac{\sinh[q(I_c-z)](B-\sqrt{B^2-1})^{|l|}}{\sqrt{B^2-1}}+\frac{\sinh(qz)(B-\sqrt{B^2-1})^{|l-1|}}{\sqrt{B^2-1}}\right\} , \tag{6}$$

where $B=\cosh(qI_c)-V_q X(q)\sinh(qI_c)/\epsilon_0$. Two interesting cases to be discussed later are with $z=0$ and $z=I_c/2$, respectively, for impurities on the graphite layers and on the intercalant layers. The induced charge density $n_l^{in}(q;z)$ is given by Eq. (6) multiplied by the response function $X(q)$. The real-space potential is obtained by the reverse Fourier transform

$$V_l^{eff}(r;z)=\frac{1}{2\pi}\int_0^\infty V_l^{eff}(q;z)J_0(qr)q\,dq , \tag{7}$$

where $J_0(qr)$ is the Bessel function of the order zero. A similar relation holds true for the induced charge density $n_l^{in}(r;z)$. We emphasize that a valid response function $X(q)$ is essential in this problem upon considering the

complicated band structure of GIC's.

The total induced charges for a good conductor like GIC's would be expected to be equal to $-Ze$. The induced charges on the lth layer are $N_l^{\rm in}(z)=V_l^{\rm eff}(q;z)X(q)$ at $q\rightarrow 0$ and can be easily evaluated by using Eq. (6). It should be noticed that there is no interband contribution since $V_q X_b(q)=0$ at $q\rightarrow 0$. The total induced charges can then be easily calculated $\sum_l N_l^{\rm in}(z)=-Z$; i.e., the sum rule is indeed satisfied. This is a good indication on the validity of our calculated dielectric function for the GIC's.

Equation (7) is ready for studying the screening properties of the stage-1 GIC's. The result is compared with that of a superlattice made of 2D electron-gas sheets (EGS). Suitable parameters are needed here for a meaningful comparison. We choose the stage-1 C_8K for this study. The method, however, can be generally applied to other stage-1 compounds. It has been measured that $E_F=1.5$ eV and $I_c=5.35$ Å for C_8K (see Table I). $\gamma_0=2.4$ eV and $\epsilon_0=2.4$ have been used here (see later discussion). As a result, the effective mass $m^*=\langle \partial^2 E(k)/\partial^2 \mathbf{k}\rangle_{\rm av}^{-1}=E_F/v_f^2=0.44m_0$, where m_0 is the bare electron mass. The same ϵ_0, I_c, and m^* are used here for the corresponding EGS. The same carrier density (N_e) and the same valley degeneracy ($g_v=2$) are kept for both of the systems. They then have the same Fermi momentum $k_F=\sqrt{N_e\pi}$. The Fermi energy of the EGS is, however, only 0.75 eV in magnitude. The two systems have the same effective Bohr radius, $a^*=\epsilon_0\hbar^2/m^*e^2=2.90$ Å, and the same $r_s=(\pi a^{*2}n)^{-1/2}=1.18$.

The static dielectric function of EGS is given by[12]

$$\epsilon_{\rm EGS}(q)=\begin{cases}\epsilon_0+S/q & \text{if } q\le 2k_F\\ \epsilon_0+S/q(1-\sqrt{1-x^{-2}}) & \text{if } q>2k_F\ ,\end{cases} \tag{8}$$

where $x=q/2k_F$ and $S=2g_v\epsilon_0/a^*$. Both Eqs. (2) and (8) can be expressed as $\epsilon(q)=\epsilon_0+q_s(q)/q$. The q-dependent screening parameter $q_s(q)$ is useful for discussion. With the chosen parameters, $q_s(0)=3.31$ Å^{-1} for both GIC's and EGS.

$q_s(q)$ are shown in Fig. 1. There are two main differences between GIC's and EGS. The first is that GIC's (the solid curve) have an important contribution from the inter-π-band transitions. It greatly enhances $q_s(q)$ in the large-q regime, especially for q between $2k_F$ and $2k_D$. If we exclude the interband transitions, i.e., putting $X_b(q)=0$, the resulting $q_s(q)$ (the dotted curve) would be even smaller than that of EGS. The second difference is in the singular behavior of $d^n q_s(q)/d^n q$. The EGS has a first-derivative singularity at $q=2k_F$. The GIC's, however, are more complicated (details in the Appendix). GIC's have a second-derivative singularity at $q=2k_F$, and have two extra singularities at $q=2k_D-2k_F$ and at $2k_D$. This is due to the finite size of the π band. It has been estimated that the band size $E_D=5.5$ eV[3] and $k_D=E_D/v_f=1.08$ Å^{-1}. The one at $2k_D$ is the most singular among the three. Very different oscillation patterns at large distances can be expected here for the two systems, since the Friedel oscillation is caused by the singularities in $d^n q_s(q)/d^n q$.

Let us first examine the $z=0$ case, for which $V_l^{\rm eff}(r;z=0)$ is plotted in Fig. 2. The screened potential on the $l=0$ plane is rather short ranged for the GIC's (the solid curves). At small r, $V_{l=0}^{\rm eff}(r;z=0)$ can be very well fitted by $6.3\exp(-1.67r)/r$ (not shown), which corresponds to a characteristic screening length of 0.6 Å. As for EGS (the dashed curves), $V_{l=0}^{\rm eff}(r;z=0)$ can be fitted by $6.5\exp(-1.25r)/r$, i.e., a longer characteristic screening length of 0.8 Å. The small-r behavior is mainly related to large-q characters of $q_s(q)$. The fact that interband transitions greatly enhance $q_s(q)$ of GIC's at $q>2k_f$ explains why $V_{l=0}^{\rm eff}$ of GIC's drops off more quickly than that of EGS. The characteristic screening length would

TABLE I. Parameters used in the calculations. We also used $\epsilon_0=2.4$ and $\gamma_0=2.4$ eV as discussed in the text.

Compounds	I_c (Å)	E_F (eV)	f (cal)	f (theo)	f (exp)
C_8K	5.35[a]	1.50	0.57	0.60[f]	0.60[i]
		1.60[b]		0.59[g]	0.84[j]
		1.40[c,d]		0.43[h]	
C_8Rb	5.65[a]	1.66	0.70	0.51[g]	0.70[j]
		1.52[e]		0.64[g]	
		1.80[d]			
C_8Cs	5.94[a]	1.23	0.38	0.30[g]	0.70[j]
		1.45[e]		0.41[h]	0.55[k]
		1.00[d]			0.5±0.2[l]
					0.30[m]

[a]Reference 1.
[b]Reference 7.
[c]Reference 15.
[d]Reference 16.
[e]Reference 17.
[f]Reference 18.
[g]Reference 6.
[h]Reference 19.
[i]Reference 20.
[j]Reference 21.
[k]Reference 22.
[l]Reference 23.
[m]Reference 24.

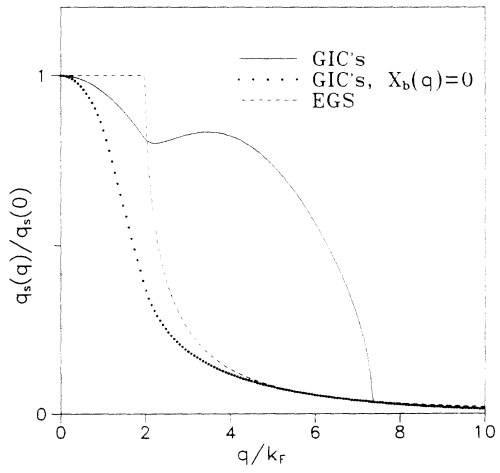

FIG. 1. The screening parameters $q_s(q)$ for GIC's (the solid curve) and for EGS (the dashed curve) are illustrated. Also shown by the dotted curve is $q_s(q)$ for GIC's, in which the contribution from the interband transitions has been neglected.

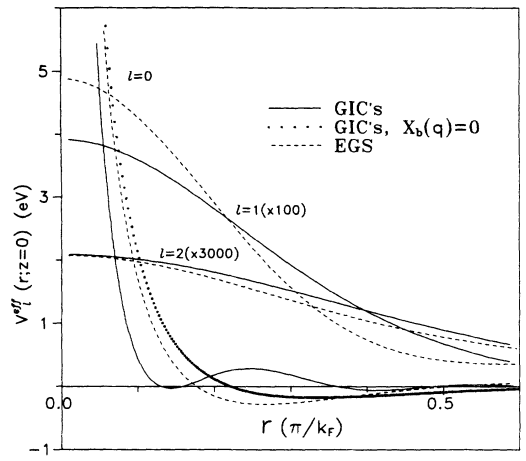

FIG. 2. The effective potentials on the planes $l=0$, 1, and 2 for a charged impurity at $z=0$. The solid curves are for GIC's, and the dashed curves for EGS. Also shown is the effective potential for GIC's if the interband transitions are neglected (the dotted curve).

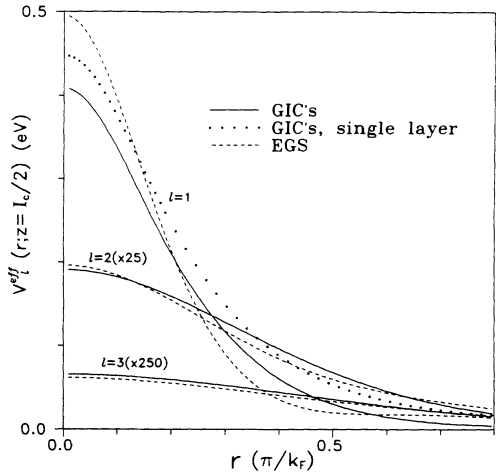

FIG. 3. Same plot as in Fig. 2, but with the charged impurity at $z=I_c/2$. The dotted curve here is, however, for a single graphite layer system; its difference with that of the GIC's demonstrates the screening effect due to the superlattice structure.

be 0.9 Å, if only the intraband transitions of the GIC's are included for calculation (the dotted curve). This is closer to that of EGS but fails badly in describing the actual GIC's.

For $l \geq 1$, the electric potentials V_l^{eff} of the two systems agree better than those in the $l=0$ case (see Fig. 2). This is mainly due to the factor $\exp(-qlI_c)$ in Eq. (6), which makes the large-q contributions less important as l grows. At $l=2$, the difference has already become negligibly small. The two should be identical as $l \to \infty$, since $q_s(0)$ has been kept the same. It also stands to reason that there would be a closer agreement in $V_{l\neq 0}^{\text{eff}}$ for the two systems if I_c increases. Their $l=0$ potential, however, would still be very different.

Next, let us put the charged impurity at $z=I_c/2$. The calculated V_l^{eff} is plotted in Fig. 3. At short distances, the $V_{l=0}^{\text{eff}}(r;z=I_c/2)$ of GIC's falls off somewhat slower than that of the EGS; the difference is much reduced if compared with the $z=0$ case. The reason is that, at $z=I_c/2$, $V_{l=0}^{\text{eff}}$ (or $V_{l=1}^{\text{eff}}$) already carries the factor $\exp(-qI_c/2)$, which makes the large-q contribution less important. For $l \geq 2$, the screened potentials of GIC's and of EGS are already very close in their size. V^{eff} of a single graphite layer with the charged impurity at $z=I_c/2$ above it (the dotted curve) is also shown in Fig. 3. The difference between this dotted curve and $V_{l=0}^{\text{eff}}$ illustrates the importance of the interlayer coupling. This effect can be enhanced by increasing z and ϵ_0, or by decreasing $q_s(0)$ and I_c. The interlayer coupling could severely affect the residual resistivity of GIC's, to be discussed later.

The induced charge distributions $N_l(r)=2\pi r n_l(r)$ for the $z=0$ case are shown in Fig. 4. Most of the screening charges on the $l=0$ plane are within the 2-Å radius around the charged impurity. $N_{l=0}(r)$ of EGS (the dashed curves) is more extended in space, and most of the screening charges are within a sphere of ~ 6 Å in radius—about three times that of GIC's. If we only consider the intraband transitions of GIC's (the dotted curve), the screening charge becomes rather extended in space. Interband transitions of GIC's greatly enhance the large-q screening (as previously studied) and consequently make the small-r screening rather effective in this system. As for the $l \geq 1$ planes, N_l^{in} of the GIC's becomes similar to that of the EGS, as can be expected from the previous discussion here.

The most outstanding feature in Fig. 4 is the strong oscillations in $N_{l=0}$ of GIC's. Such Friedel oscillations of GIC's behave very differently from that of EGS. For

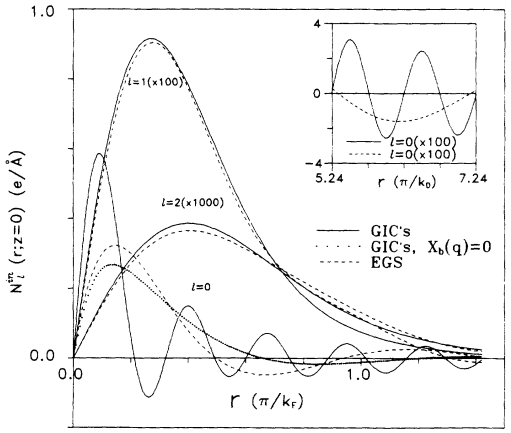

FIG. 4. The induced charge distributions on the planes $l=0$, 1, and 2 are plotted as functions of π/k_F for a charged impurity at $z=0$. The solid curves are for GIC's, and the dashed curves for EGS. The dotted curve is also the charge distribution on the $l=0$ plane of the GIC's but with the exclusion of the interband transitions. The inset shows the strong Friedel oscillation at large r on the $l=0$ plane is due to the singularity at $2k_D$. Note that the horizontal scale is π/k_D for the inset.

EGS, the oscillations on all planes are described by $\sin(2k_F r)/r^2$ at large r; i.e., a fixed oscillation period of π/k_F exists. Three derivative singularities exist for GIC's at $2k_F$, $2k_D-2k_F$, and $2k_D$, and their relative strength is l dependent. The oscillation on the $l=0$ plane is dominated by the singularity at $2k_D$. This explains the strong, rapid oscillation with the period of $\pi/k_D=2.8$ Å (see the inset). The oscillation at this wavelength diminishes rapidly for $l\geq 1$ because of the $\exp(-2k_D l I_c)$ factor involved. The main feature on the $l=1$ plane is a weaker oscillation (not shown) with the period of π/k_F.

The strong, short-wavelength oscillations in $N_{l=0}^{\text{eff}}$ deserve a closer examination. The singularity at $2k_D$ is due to the finite size of the π bands: the Blinowski's band structure, Eq. (1), has been cut off abruptly at k_D in order to conserve the particle number.[3] The singular behavior and the corresponding oscillations might have been exaggerated. A singularity at $q\sim 2k_D$, however, seems inevitable since the π band is actually finite in size. Whether this singularity is to cause a strong oscillation requires further investigation. A strong Friedel oscillation of short wavelength might affect, e.g., correlations between impurities.

The induced charge distributions with $z=I_c/2$ are shown in Fig. 5. The induced charge distributions for the two systems appear similar in shape at small r. This is due to the $\exp(-qI_c/2)$ factor which makes the large-q difference (Fig. 1) less important, as was previously explained for Fig. 3. A rather interesting oscillation pattern exists on the $l=1$ layer of GIC's for large r. The details are shown in the inset. This has been identified as being caused by the two competing oscillations with the respective wavelengths of π/k_F and π/k_D. The same factor $\sim\exp(-qI_c/2)$ puts different weights on the two singularities at $q=2k_F$ and $2k_D$. This, as a result, makes their corresponding oscillations comparable in strength

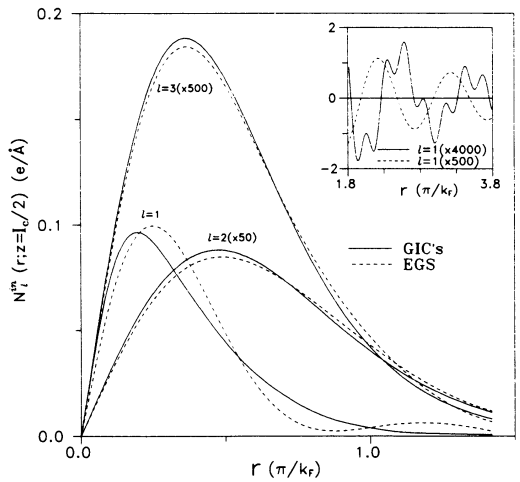

FIG. 5. Same plot as in Fig. 4, but for the $z=I_c/2$ case. The inset shows the large distance Friedel oscillation on the $l=1$ plane. Two competing oscillations with the wavelengths π/k_F and π/k_D, respectively, exist.

in the present case. The oscillations on other layers are found to be dominated by the singularity at $q=2k_F$.

The special oscillation pattern revealed in Fig. 5 is significant in that the oscillations of π/k_F may be adjusted by varying the Fermi-level energy, while the other one (π/k_D) is essentially fixed by the structure. The two competing oscillations may then be made with commensurable (or incommensurable) periods by employing suitable intercalants. The effects that such complicated screening profiles have, e.g., on the ordering of intercalants, need to be closely investigated in the future.

For the $z=0$ case, the induced charge on the lth plane is $N_l^{\text{in}}(z=0)=-\sqrt{(b-1/b+1)}\{b-\sqrt{b^2-1}\}^{|l|}$, where $b=1+q_s(0)I_c/\epsilon_0\approx 8.38$, and the induced charge ratio of two neighboring planes is $(b-\sqrt{b^2-1})\approx 0.06$. Therefore, 89% of the induced charges are on the $l=0$ plane, and the remaining 11% are mostly on the $l=\pm 1$ planes. For $z=I_c/2$, the induced charge ratio is also given by $(b-\sqrt{b^2-1})$—with the exception of $l=0$ and 1 planes: 94% of the induced charges are equally distributed on these two planes.

The essential features of the screened potential are not expected to differ qualitatively for other GIC's, which might have different I_c, E_F, ϵ_0, and γ_0. The screening properties of GIC's are essentially shaped by the band of graphite and the periodic superlattice structure.

III. THE RESIDUAL RESISTIVITY

We now employ the relations established in the previous section to calculate the residual resistivity due to charged impurities. From measured residual resistivities we estimate that the impurity density in the stage-1 GIC's is about 10^{-4} per intercalation atom. The same impurity concentration, however, is found to be insufficient in accounting for the residual resistivity found in the stage-2 GIC's.

The Boltzmann equation within the relaxation-time approximation is employed here for evaluating the resistivity. The current density $\mathbf{J}$ is then found to be

$$\mathbf{J}\equiv\rho^{-1}\mathbf{E}=[I_c m^*/N_e e^2\tau(k_F)]^{-1}\mathbf{E}\ . \tag{9}$$

N_e is the 2D conduction electron density. The special band structure of GIC's [i.e., Eq. (1)] has been employed in deriving this result, so that $m^*=E_F/v_f^2$ and $N_e=k_F^2/\pi$. The double-valley degeneracy has also been included. The resistivity ρ of Eq. (9) has the usual form of $I_c m^*/N_e e^2\tau$, despite the very complicated band structure involved.

The impurity distribution needs to be specified here in order to evaluate $\tau(k_F)$, so that the resistivity can be then determined via Eq. (9). We assume that impurities are either all on the graphite layers ($z=0$) or all on the intercalant layers ($z=I_c/2$) with an averaged 2D impurity density N_{im}. The present calculation can be easily generalized for other impurity distributions. With N_{im} given, the relaxation time is expressed by

$$1/\tau(k_F)=(N_{\text{im}}k_F^2/\pi E_F)\int_0^{\pi}d\theta|T_{kk'}|^2(1-\cos\theta)_{|k=k'=k_F}\ , \tag{10}$$

where θ is the angle between $\mathbf{k}$ and $\mathbf{k}'$. The scattering matrix element $T_{kk'}$ within the Born approximation, is given by $T_{kk'}=\sum_q V^{\rm eff}(q;z)\langle\Psi^c_{k'}(\mathbf{r})|e^{i\mathbf{q}\cdot\mathbf{r}}|\Psi^c_k(\mathbf{r})\rangle$, where $z=0$ or $z=I_c/2$. The intervalley and the umklapp processes have been neglected here since they involve a large momentum transfer and are, hence, negligible. With the use of the realistic Bloch wave functions[3] for GIC's, it is found that $(\mathbf{k}'-\mathbf{k}=\mathbf{q})$

$$T_{kk'}|_{k=k'=k_F}=\tfrac{1}{2}I(q)V^{\rm eff}(q;z)(1+\cos\theta-i\sin\theta)\ , \qquad (11)$$

where $I(q)=[1+(q/6)^2]^{-3}$. It is interesting to note that $|T_{kk'}|^2\sim(1+\cos\theta)$, which cancels the familiar enhancement factor for the backward scattering: $[1-\cos(\theta)]$ in Eq. (10). This unusual property is caused by the special band structure of the system and has been explored before.[13] This factor alone could reduce the resistivity of GIC's by a factor of ~ 2. The angle factors in Eqs. (10) and (11) make $\theta=\pi/2$ the most relevant scattering angle in evaluating $1/\tau(k_F)$. It is clear from this discussion that we cannot expect to quantitatively study the system without addressing its band-structure effect.

Substituting Eqs. (10) and (11) back to (9), we obtain

$$\rho=\frac{2I_c k_F^4}{\pi E_F^2}\frac{N_{\rm im}}{N_e}\int_0^{\pi/2}d\theta\sin^2(2\theta)I^2(q) \times|V^{\rm eff}(q;z)|^2_{|q=2k_F\sin\theta}\ . \qquad (12)$$

Here, the resistivity is in units of $\text{Å}/e^2$. One may simply multiply the result by 36 to convert it to $\mu\Omega$ cm, which could be more convenient to use. The l-independent effective potential $V^{\rm eff}(q;z)$ in Eq. (12) is the effective potential due to all impurities. In terms of $V_l^{\rm eff}(q;z)$, one can express $|V^{\rm eff}(q;z)|^2=\sum_l|V_l^{\rm eff}(q;z)|^2$ and evaluate the summation exactly,

$$|V^{\rm eff}(q;z)|^2=\frac{Z^2V_q^2(B\{\sinh^2[q(I_c-z)]+\sinh^2(qz)\}+2\sinh(qz)\sinh[q(I_c-z)])}{\epsilon_0^2(B^2-1)^{3/2}}\ . \qquad (13)$$

An attempt has been made to estimate the residual resistivity for the C_8M compounds. Investigating if the measured residual resistivities could be reasonably explained with the charged impurity scattering is the purpose of this calculation. For lack of detailed information about the impurities, $Z=1$ is assumed here for the impurities and they are put either all on the graphite layers or all on the intercalant layers. Such configurations seem appropriate for an order estimation. Also, we put $\epsilon_0=2.4$;[14] i.e., we neglect the modification of the background dielectric constant due to intercalants. These assumptions can be easily modified once the nature of impurities and of intercalants have been more clearly specified.

For the rigid Blinowski's band structure, E_F and the charge transfer are relafed by $E_F=\gamma_0(\sqrt{3}\pi f/p)^{1/2}$, where f represents the charge transferred to the π band per donor atom and $p=8$ for the C_8M compounds. The measured E_F is used here as the input in our calculation. The measured values unfortunately fluctuate widely: Take C_8Cs, for example, with an E_F range from 1.0 to 1.45 eV. Their simple averages are taken as our input E_F, since no obvious way exists for choosing from the scattered data. The practice seems appropriate for our qualitative discussion presented below. Input parameters are summarized in Table I. The calculated f are in reasonable agreement with other reported values.

Our results are summarized in Table II. We have used Eq. (12) and measured resistivity to estimate the impurity density for each compound with impurities either at $z=0$ or $z=I_c/2$. The density, expressed by $N_{\rm im}/I_c$, suggests the convenient units $n_{\rm im}=10^{-6}$ Å^{-3}. For C_8M, which has $I_c\simeq 5.5$ Å, $1n_{\rm im}$ means 10^{-5} impurities per carbon atom if $z=0$, and $1n_{\rm im}$ would suggest 10^{-4} per intercalated atom if $z=I_c/2$.

These results most noticeably suggest a rather low charge impurity density at approximately $1n_{\rm im}$ for all cases. Such impurity density is even considered low for graphite single crystals. For example, the K and Rb results with $z=0$ suggest an impurity concentration of about $0.5n_{\rm im}$. If the intercalated compounds are made from 99.995% pure graphite[25] with all the impurities charged ones, these impurities alone would be sufficient to explain the observed resistivity. The relatively higher impurity level for the Cs compounds seems to indicate that extra impurities are introduced to the system during the intercalation.

Our theory has also been modified for stage-2 compounds. An impurity density of about $10n_{\rm im}$ was found to be necessary in order to explain the measured resistivity (0.25 $\mu\Omega$ cm) of the $C_{24}K$.[26] It seems unlikely that the stage-2 compounds would have an order of magnitude more impurities than the stage-1 compounds had. This result suggests that other mechanisms, e.g., the domain wall scattering,[2,27] might be more important in stage-2 compounds.

In short, the present calculations provide a strong indication that charged impurity scattering is essential in causing electric resistivity for stage-1 GIC's, but probably

TABLE II. Measured in-plane resistivity ($\rho_{\rm exp}$) and the calculated impurity density ($n_{\rm im}$). $n_{\rm im}$ is in the unit of 10^{-6} Å^{-6}.

Compounds	$\rho_{\rm exp}$[a] ($\mu\Omega$ cm)	$n_{\rm im}$ ($z=0$)	$n_{\rm im}$ ($z=I_c/2$)
C_8K	8.36×10^{-3}	0.52	2.34
C_8Rb	9.66×10^{-3}	0.56	3.73
C_8Cs	4.06×10^{-2}	2.01	5.73

[a]Reference 10.

not for stage-2 GIC's. Equations (12) and (13) actually enable us to analyze this problem quantitatively—provided that the nature of impurities are known closely.

IV. CONCLUDING REMARKS

In this work, we have studied the screening properties of GIC's and calculated the residual resistivity for the C_8M compounds. The band structure of GIC's has several unique features: the valence band and the conduction band are degenerate in energy at the U point, are linear in the energy dispersion relation, and have finite sizes. The systems are also highly anisotropic: it is a layer system. Including these features in the dielectric function is important; we achieve this by employing Shung's dielectric function, which analytically takes into account these unique structures of GIC's.

The closeness in the energy of the valence and the conduction bands makes it necessary to include both bands in the calculation. The strong interband transitions were found to have greatly enhanced the screening at short distances. The finite size of the bands, however, causes a strong and rapid Friedel oscillation at large distances from an impurity. Such an oscillation is expected to affect the impurity ordering. A closer investigation in this regard is needed.

The linear energy dispersion is found to have important effects on the mobility of electrons. It reduces the effective mass of electrons, and leads to a vanishing backward-scattering amplitude. This practically explains the excellent conductivity of GIC's. The residual resistivities of the C_8M compounds have been calculated and the results compared with the measurements. A small amount of charged impurities has been found to be sufficient in explaining the measured resistivity. However, this part of study is not quantitatively conclusive, since the nature of the impurities is not clearly known. It should be possible to examine this problem closely, e.g., by doping impurities into GIC's in a controlled manner.

This study has illustrated the importance the unique structure has on the screening of GIC's. A dielectric function has been employed here that is calculated in accordance with the band structure of GIC's and is good to within the random-phase approximation and analytic in form. This method provides a basis for further investigation on screening-related properties of the layered graphite compounds.

ACKNOWLEDGMENTS

This work was supported in part by the National Science Council of the Republic of China under Grant No. NSC 81-0208-M007-09.

APPENDIX

The response functions of the GIC's, and their singularities are summarized here. Both intraband and interband excitations exist in the system. For the intraband transitions, the response function $X_a(q)$ is[3] ($E_q=v_f q$)

$$X_a(q)=\frac{-q^2I^2(q)}{2\pi^2}\int_0^{E_q}\frac{F(w)-F(-w)}{w\sqrt{E_q^2-w^2}}dw\ , \tag{A1}$$

where

$$F(w)=\Theta[T(w)-1]\{T(w)\sqrt{T^2(w)-1}-\ln[T(w)+\sqrt{T^2(w)-1}]\}\ , \tag{A2}$$

and

$$T(w)=\frac{2E_F+w}{E_q}\ . \tag{A3}$$

$X_a(q)$ has a second-derivative singularity at $q=2k_F$. The singularity at $q=2k_F$ is due to the presence of a filled Fermi sea as in the case of an electron-gas system. The difference is that the singularity for the electron gas is a first-derivative one. The cause for this difference can be understood from their response functions. For GIC's, we found[3]

$$X_a(q)=2I^2(q)\sum_{\mathbf{k}}\frac{f^0(E_{k+q})-f^0(E_k)}{E_{k+q}-E_k}\times\left\{1+\frac{k+q\cos(\psi)}{|\mathbf{k}+\mathbf{q}|}\right\}\ , \tag{A4}$$

where ψ is the angle between $\mathbf{k}$ and $\mathbf{q}$. The Coulomb interaction, due to the special linear π band of GIC's, contains the factor expressed inside the curly bracket. The corresponding factor would be one for the electron gas. The singularity at $q=2k_F$ corresponds to excitations from states at $|\mathbf{k}|=|\mathbf{k}+\mathbf{q}|=k_F$, i.e., when $\psi=\pi$. The factor becomes zero at the singularity and, as a result, the singularity for GIC's has a reduced strength.

The response function for the interband transitions is[3]

$$X_b(q)=2[H_1(q)+H_2(q)]\ , \tag{A5}$$

where

$$H_1(q)=\frac{-I^2(q)q^2}{2\pi^2E_q}\int_{\theta_3}^{\theta_4}[\theta_c-0.5\sin(2\theta_c)]d\theta\ , \tag{A6}$$

$$H_2(q)=\frac{-I^2(q)qk_F}{4\pi E_F}(\theta_2-\theta_1)\ , \tag{A7}$$

and

$$\theta_c=\arccos\left[\left[\frac{2E_F}{E_q}\right]-\sec(\theta)\right]\ ,$$

$$\theta_1=\arccos\left[\frac{E_q}{2E_F+E_q}\right]\ ,$$

$$\theta_2=\arccos\left[\frac{E_q}{2E_D}\right]\ ,$$

$$\theta_3=\begin{cases}\arccos\left[\dfrac{E_q}{2E_F-E_q}\right] & \text{if } E_F>E_q\\ 0 \text{ if } E_F<E_q\ ,\end{cases}$$

$$\theta_4 = \begin{cases} \arccos\left[\dfrac{E_q}{2E_F+E_q}\right] & \text{if } E_q < 2E_D - 2E_F \\ \arccos\left[\dfrac{E_q}{2E_D}\right] & \text{if } E_q > 2E_D - 2E_F \ . \end{cases}$$

$H_2(q)$ is a well-behaved function within $q=2k_D-2k_F$. $H_1(q)$ has first-derivative discontinuities at $q=2k_D-2k_F$ and at $2k_D$. These singularities are caused by the finite size of the π band, and they are the most singular ones for the GIC's.

[1]M. S. Dresselhaus and G. Dresselhaus, Adv. Phys. **30**, 139 (1981); M. S. Dresselhaus, *Intercalation in Layered Materials* (Plenum, New York, 1987).

[2]R. S. A. Safran, Solid State Phys. **40**, 183 (1987).

[3]K. W.-K. Shung, Phys. Rev. B **34**, 979 (1986).

[4]P. R. Wallace, Phys. Rev. **71**, 622 (1947); J. Blinowski, Nguyen Hy Hau, C. Rigaux, J. P. Vieren, R. Le. Toullee, G. Furdin, A. Herold, and J. Melin, J. Phys. (Paris) **41**, 47 (1980); J. Blinowski and C. Rigaux, *ibid.* **41**, 667 (1980).

[5]K. W.-K. Shung, Phys. Rev. B **34**, 1264 (1986).

[6]P. Alstrom, Synth. Metals **15**, 311 (1986).

[7]G. L. Doll, M. H. Yang, and P. C. Eklund, Phys. Rev. B **35**, 9790 (1987); D. M. Hoffman, R. E. Heinz, G. L. Doll, and P. C. Eklund, *ibid.* **32**, 1278 (1985).

[8]D. P. DiVincenzo and E. J. Mele, Phys. Rev. B **29**, 1685 (1984).

[9]L. Pietronero, S. Strassler, and H. R. Zeller, Phys. Rev. Lett. **41**, 763 (1978).

[10]M. E. Potter, W. D. Johnson, and J. E. Fischer, Solid State Commun. **37**, 713 (1981).

[11]A. C. Teslis and J. J. Quinn, Phys. Rev. B **29**, 3318 (1984).

[12]F. Stern, Phys. Rev. Lett. **18**, 546 (1967).

[13]S. E. Ulloa and G. Kirczenow, Phys. Rev. B **35**, 795 (1987).

[14]E. A. Taft and H. R. Philipp, Phys. Rev. **138**, A197 (1965).

[15]J. J. Ritsko, Phys. Rev. B **25**, 6452 (1982).

[16]P. Oelhafen, P. Pfluger, E. Hauser, and H.-J. Guntherodt, Phys. Rev. Lett. **44**, 197 (1980).

[17]L. A. Grunes and J. J. Ritsko, Phys. Rev. B **28**, 3439 (1983).

[18]T. Ohno, K. Nakao, and H. Kamimura, J. Phys. Soc. Jpn. **47**, 1125 (1979); H. Kamimura, K. Nakao, T. Ohno, and T. Inoshita, Physica B **99**, 401 (1980).

[19]L. Pietronero and S. Strassler, Phys. Rev. Lett. **47**, 593 (1981).

[20]T. Takahashi, N. Gunasekara, T. Sagawa, and H. Suematsu, J. Phys. Soc. Jpn. **55**, 3498 (1986).

[21]J. Conard, H. Estrade, P. Lauginie, H. Fuzellier, H. Furdin, and R. Vasse, Physica B **99**, 521 (1980).

[22]G. P. Carver, Phys. Rev. B **2**, 2284 (1970).

[23]L. E. Campbell, G. L. Montet, and G. J. Perlow, Phys. Rev. B **15**, 3318 (1977).

[24]G. Roth, K. Luders, P. Pfluger, and H.-J. Guntherodt, Solid State Commun. **39**, 423 (1981).

[25]D. E. Soule, Phys. Rev. **112**, B698 (1958).

[26]D. G. Onn, G. M. T. Foley, and J. E. Fischer, Phys. Rev. B **19**, 6474 (1979).

[27]N. Daumas and A. Herold, C. R. Acad. Sci. Ser. C **268**, 373 (1969).